International Scientific Journal of Engineering and Management (ISJEM) ISSN: 2583-6129
Volume: 05 Issue: 01 | Jan – 2026 DOI: 10.55041/ISJEM05344
An International Scholarly || Multidisciplinary || Open Access || Indexing in all major Database & Metadata

An Enhanced Solar Power Generation System for Power Smoothing and Output Stability and Temperature Monitoring using IOT

1. Mr. Krishna Govind Chavan
Zeal College of Engineering, Research. Pune
Contact Us - Zeal College of Engineering and Research
Krishnachavan0987@gmail.com Researched By.

2. Prof. Dhirendra Deode
Zeal College of Engineering, Research. Pune
Contact Us - Zeal College of Engineering and Research

3. Dr. Anagha Soman
Zeal College of Engineering, Research. Pune
Contact Us - Zeal College of Engineering and Research

Abstract— **The output power of a solar power generation system (SPGS) can fluctuate significantly due to environmental factors, impacting the stability and reliability of the power distribution network. To address this, a new SPGS design with a built-in power smoothing function is proposed. The system includes a solar cell array, a battery pack, a dual-input buck-boost DC-AC inverter (DIBBDAI), and a boost power converter (BPC). The DIBBDAI handles voltage boosting, bucking, and DC-AC conversion within a single unit, while the BPC serves as a battery charger between the solar cell array and the battery pack. In this setup, DC power from either the solar array or the battery is directly converted into AC power through a single-stage process, enhancing the overall power conversion efficiency. Similarly, the solar array charges the battery through a single-stage conversion. This streamlined approach improves energy efficiency across the solar array, the battery system, and the grid. To mitigate the effects of sudden changes in solar output, the battery charges or discharges as needed, helping to smooth the system's power output. Additionally, the DIBBDAI reduces leakage currents caused by the parasitic capacitance of the solar array. Overall, the proposed interface not only boosts power efficiency and stabilizes power output but also minimizes leakage current in the SPGS. A hardware prototype has been developed and tested to validate the system's performance.**

Keywords— Solar power generation, power smoothing, buck-boost DC-AC inverter.

I. INTRODUCTION

Extreme climate change and global warming have driven international efforts to reduce greenhouse gas emissions, led by United Nations initiatives. As a result, many countries are rapidly adopting renewable energy sources, particularly solar and wind power, which are now supported by mature technologies. Advances in manufacturing have significantly reduced costs, making renewable electricity comparable to or cheaper than fossil-fuel-based generation. Consequently, large numbers of renewable power systems are being integrated into power grids worldwide.

The output power of a solar power generation system (SPGS) varies significantly due to uncontrollable environmental factors such as weather and seasonal changes [1]–[12]. As SPGS penetration increases, these fluctuations can adversely affect grid voltage, frequency, and overall power quality, potentially leading to outages. Existing control strategies mainly limit upward power variations by sacrificing maximum power point tracking, which reduces energy yield and fails to address downward fluctuations [1]. Therefore, rapid power regulation using temporary energy storage is essential.

Battery energy storage systems (BESS) are well suited for power smoothing because of their fast response, compact size, and flexible operation [2]–[16]. Typically, the BESS compensates for the difference between the average and instantaneous SPGS output power. Average power is commonly obtained using low-pass filters, moving average filters, Savitzky–Golay filtering, or moving regression methods [3]–[9]. However, since instantaneous power rarely equals its average, batteries often experience long charge and discharge durations.

Because both solar arrays and batteries operate in DC, a DC-AC power conversion interface is required for grid connection [1]–[23]. SPGS-BESS configurations are classified into AC-coupled [9]–[12] and DC-coupled [4], [8], [13]–[16] systems. AC coupling requires separate converters for the SPGS and BESS, increasing complexity, while DC coupling shares a common inverter and offers a simpler structure. However, in low-voltage systems, additional boost converters are required to meet grid voltage levels, increasing conversion stages, reducing efficiency, and complicating circuit design.

Several advanced DC-AC converter topologies have been proposed, including Z-source inverters [19], [20], [24], [25], boost DC-AC converters [26], [27], and buck-boost-based architectures [28]–[32]. Although these approaches provide voltage boosting capability, they suffer from limitations such as increased switching loss, complex control, leakage current issues, reduced efficiency, or the ability to process only a single DC source.

To address these challenges, this study proposes an SPGS with a power smoothing function based on a dual-input buck-boost DC-AC inverter (DIBBDAI) combined with a boost power converter (BPC). The proposed system integrates both a solar cell array and a battery set. All grid-connected AC

power conversion is performed using the DIBBDAI, while the BPC is used solely to charge the battery from the solar array. The battery charges or discharges in response to rapid solar power variations, effectively smoothing the SPGS output. Additionally, the proposed configuration reduces high-frequency voltage components at the solar array terminal, thereby minimizing leakage current.

II. RELATED WORK

Peng et al. (2020) proposed a grid-friendly control strategy for smart PV systems that dynamically regulates active and reactive power to support grid stability. Their method adapts to rapid irradiance variations and improves grid resilience while maintaining high PV efficiency. However, the study focused mainly on control algorithms and did not incorporate energy storage, leaving sudden power drops from fast weather changes insufficiently mitigated.

Cheng et al. (2016) investigated the effects of very high PV penetration on distribution networks and showed that increased PV integration can lead to voltage instability, back-feeding, and frequency issues. Using both simulations and real data, they demonstrated that even short-term irradiance fluctuations can degrade grid reliability. Their solutions emphasized advanced grid-level management but gave limited attention to local PV-side power smoothing.

Martins et al. (2019) compared several ramp-rate control methods for PV systems with energy storage, including conventional filters and PID-based controllers. While most approaches reduced power fluctuations, they often affected battery life or system responsiveness. The study concluded that optimal control depends on system and environmental conditions, though it did not explore alternative hardware or inverter architectures.

Lin (2020) reviewed multiple ramp-rate mitigation techniques, including curtailment and storage-based smoothing, highlighting the use of moving average and low-pass filters. Although these methods are simple to implement, they require frequent tuning and may underperform during rapid weather changes. The work supported storage integration but lacked discussion on converter-level implementation.

Nazaripouya et al. (2018) introduced a two-stage optimization-based filtering approach for battery energy storage to smooth PV output. The method balanced fast response with energy efficiency and achieved effective smoothing. However, its computational complexity and lack of inverter-level design details may limit real-time, cost-effective deployment.

Koiwa et al. (2018) analyzed filter design for energy storage systems, focusing on the trade-off between smoothing quality and battery size. Their results showed that stricter frequency control demands larger storage capacity, increasing cost. While the study advanced theoretical understanding, it remained confined to control strategies without proposing practical system architectures.

Alam et al. (2014) proposed a predictive ramp-rate control strategy using irradiance forecasting and battery support. The approach enabled proactive smoothing and outperformed basic filtering methods, but its effectiveness depended heavily on forecast accuracy, making it less reliable under rapidly changing weather conditions.

Atif and Khalid (2020) demonstrated that Savitzky–Golay filtering can improve PV power smoothing while preserving signal characteristics and limiting excessive battery usage. Despite promising results, the method relied on continuous signal processing and did not address converter-level efficiency or hardware integration challenges.

Syed and Khalid (2021) presented an adaptive moving regression filter combined with battery SOC feedback to enhance PV firming and extend battery life. While effective in ramp-rate control, their approach used a conventional multi-stage conversion structure, which may reduce overall system efficiency due to additional power losses..

III. CIRCUIT CONFIGURATION

The circuit configuration of the proposed SPGS is illustrated in Fig. 1. A DC-coupled structure is adopted, comprising a solar cell array, a battery set, and a power conversion interface. The power conversion interface includes a DIBBDAI and a BPC. The BPC is placed between the solar cell array and the battery set to regulate the charging power. To minimize the required battery capacity, the battery operates only when the power variation of the solar cell array exceeds a predefined limit. Since the battery is charged exclusively by the solar array, the BPC enables unidirectional power flow.

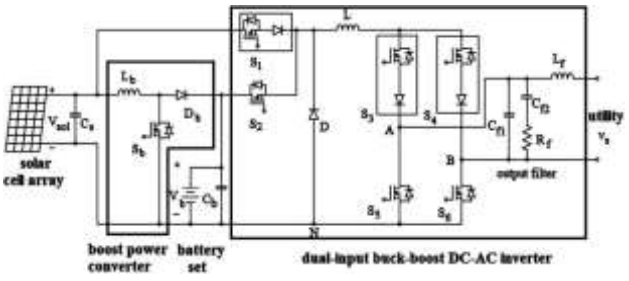

FIGURE 1. Circuit configuration for the proposed SPGS

The DIBBDAI provides voltage boost, voltage buck, and DC–AC conversion. Both the DIBBDAI and BPC operate simultaneously, allowing the solar array to supply power to the grid while charging the battery set.

IV. OPERATION OF DIBBDAI

The two input terminals of the DIBBDAI are connected to the solar cell array and the battery set. Its operation is classified into boost and buck modes. Switches S1 and S2 are linked to the respective input terminals. Since the solar array voltage is lower than the battery voltage, S1 includes a diode to form a unidirectional switch, preventing reverse voltage from the battery. During buck operation, S1 and S2 function as controlled switches.

In the proposed SPGS, the solar array and battery do not supply power simultaneously; therefore, S1 and S2 never operate at the same time. The DIBBDAI also employs a bridge formed by switches S3–S6 to generate AC output current. Switches S3 and S4 include diodes to prevent grid short circuits and also act as switches in boost mode. Components Cf1, Cf2, Rf, and Lf constitute a damped second-order low-pass filter.

When the solar array is active and the battery is inactive, S1 is turned on while S2 remains off. If the grid provides two DC input terminals connected to the battery and solar array, both sources can independently use the DIBBDAI to deliver AC power to the grid.

Under stable solar output, power is supplied directly to the grid through the DIBBDAI, the BPC is disabled, and the battery remains in standby. When solar power drops suddenly, the battery supplies power to the grid while the BPC tracks the maximum solar power to charge the battery. Conversely, when solar power increases and the DIBBDAI output voltage is lower than the solar voltage, the converter operates in buck mode. In this mode, S1 is PWM-controlled, while S3–S6 switch according to grid voltage polarity. Buck operation consists of four modes.

Mode Bk-1: During the positive grid voltage half cycle, S1, S3, and S6 are on, while S4, S5, and D are off. The inductor current change rate is:

$$\frac{di_L}{dt} = \frac{V_{sol} - v_s}{L} \quad (1)$$

where vs and $Vsol$ denote the grid voltage and the solar array voltage, respectively. In this interval, the solar array transfers energy to the inductor and then to the grid.

Mode Bk-2: During the positive half cycle of the grid voltage, switches S3 and S6 along with diode D are ON, while S1, S4, and S5 are OFF. Under this condition, the rate of change of the inductor current is given by:

$$\frac{di_L}{dt} = -\frac{v_s}{L} \quad (2)$$

The inductor supplies energy to the grid.
Mode Bk-3: In the negative half-cycle of the grid voltage, switches S1, S4, and S5 are ON, while S3, S6, and D are OFF. The inductor current changes at the rate:

$$\frac{di_L}{dt} = \frac{V_{sol} + v_s}{L} \quad (3)$$

The solar cell array supplies energy to both the inductor and the grid.
Mode Bk-4: During the negative half cycle of the grid voltage, switches S4 and S5 and diode D conduct, while S1, S3, and S6 remain off. Under this condition, the rate of change of the inductor current is given by:

$$\frac{di_L}{dt} = -\frac{v_s}{L} \quad (4)$$

The inductor transfers stored energy to the grid. Figure 2 shows the equivalent circuit of the DIBBDAI operating in buck mode, where S corresponds to S1. Switches S3–S6 convert the grid voltage to its absolute value and combine it with the output of a conventional buck converter. Thus, the DIBBDAI behaves like a standard buck converter, and the inductor current is regulated through the switching of S.

When the grid voltage exceeds the solar array voltage, the DIBBDAI operates in boost mode. In this case, S1 remains continuously on, while S3–S4 are PWM-controlled during the positive and negative grid half cycles, respectively, and S5–S6 switch according to grid polarity. Boost operation is divided into four modes. In Mode Bt-1, during the positive half cycle, S3, S4, and S6 are on and S5 is off, determining the rate of change of the inductor current.

$$\frac{di_L}{dt} = \frac{V_{sol}}{L} \quad (5)$$

The solar cell array transfers energy to the inductor.
Mode Bt-2: During the positive half cycle of the grid voltage, switches S3 and S6 are ON, while S4 and S5 are OFF. Under this condition, the rate of change of the inductor current is given by:

$$\frac{di_L}{dt} = \frac{V_{sol} - v_s}{L} \quad (6)$$

Both the solar array and the inductor supply energy to the grid.
Mode Bt-3: During the negative half cycle of the grid voltage, switches S3, S4, and S5 are turned on, while S6 remains off. Under this condition, the inductor current varies at the following rate:

$$\frac{di_L}{dt} = \frac{V_{sol}}{L} \quad (7)$$

The solar cell array releases energy to the inductor.

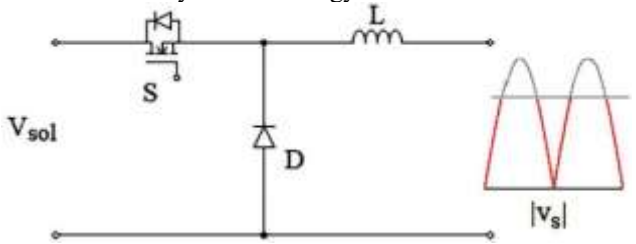

FIGURE 2. Equivalent circuit for the DIBBDAI in the buck mode.

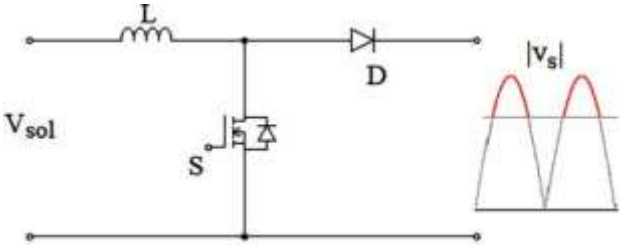

FIGURE 3. Equivalent circuit for the DIBBDAI in the boost mode.

International Scientific Journal of Engineering and Management (ISJEM) ISSN: 2583-6129
Volume: 05 Issue: 01 | Jan – 2026 DOI: 10.55041/ISJEM05344
An International Scholarly || Multidisciplinary || Open Access || Indexing in all major Database & Metadata

Mode Bt-4: When the grid voltage is in the negative half cycle, S4 and S5 are turned on and S3 and S6 are turned off. The change rate for the inductor current is:

$$\frac{di_L}{dt} = \frac{V_{sol} + v_s}{L} \quad (8)$$

Both the solar cell array and the inductor deliver energy to the grid. Figure 3 shows the equivalent circuit of the DIBBDAI in boost mode. The grid voltage is rectified to its absolute value and added to the output of the conventional BPC through switches S3–S6. Depending on the grid voltage polarity, S3 or S4 acts as the active switch, and the corresponding body diode conducts. In this mode, the DIBBDAI behaves like a conventional BPC, with the inductor current regulated by the active switch.

When powered by the battery set, S2 is turned on and S1 is turned off, and the DIBBDAI operates in the same manner as in the solar-powered case; hence, this operation is not repeated. The switching states of S1–S6 are summarized in Table 1, where PHC and NHC denote the positive and negative half cycles. Figure 4 illustrates the control signals and operating voltages over one grid cycle, showing that only one switch operates with PWM at a time, while VAN and VBN closely follow the positive and negative grid voltages, respectively.

Figure 5 presents the equivalent circuit used for leakage current analysis [33], [34]. Here, Cpv represents the parasitic capacitance of the solar array and Rg the grid ground resistance. Voltages VAN and VBN are measured from terminals A and B to the negative terminal N of the solar array. Since $Cf1$, $Cf2$, and Rf are connected across A and B, they do not influence the leakage current. Switches S5 and S6 operate synchronously with the grid voltage: S6 conducts and S5 is off during the positive half cycle, and vice versa during the negative half cycle.

$$V_{AN} = v_s + v_{Lf} \quad (9)$$

$$V_{BN} = 0 \quad (10)$$

where vLf is the voltage of Lf. Since VBN is equal to 0, the voltage across the loop of CPV and Rg is 0 and the leakage current is 0.
When the grid voltage is in the negative half cycle, S5 is turned on and S6 is turned off and

$$V_{AN} = 0 \quad (11)$$

$$V_{BN} = -(v_s + v_{Lf}) \quad (12)$$

The voltage across the CPV–Rg loop is −(vs + vLf). Since vs is a 60 Hz sinusoidal signal and the stray capacitor has very high impedance at this frequency, the resulting leakage current from vs is negligible.

TABLE 1. Operation of S1-S6.

	power source	voltage range	S_1	S_2	S_3	S_4	S_5	S_6
PHC	solar cell array	$v_S<V_{sol}$	PWM	off	on	off	off	on
		$v_S>V_{sol}$	on	off	on	PWM	off	on
	battery	$v_S<V_b$	off	PWM	on	off	off	on
		$v_S>V_b$	off	on	on	PWM	off	on
NHC	solar cell array	$\|v_S\|<V_{sol}$	PWM	off	off	on	on	off
		$\|v_S\|>V_{sol}$	on	off	PWM	on	on	off
	battery	$\|v_S\|<V_{sol}$	off	PWM	off	on	on	off
		$\|v_S\|>V_{sol}$	off	on	PWM	on	on	off

Although vLf includes switching-frequency components due to output current ripple, these components are effectively attenuated by Cf1, Cf2, and Rf. As shown in Fig. 4(g) and (h), VAN and VBN closely follow the positive and negative grid voltages, respectively, which agrees with the analysis. Consequently, even though the stray capacitor impedance is low at the switching frequency, the leakage current induced by vLf remains small, consisting of only minor switching-frequency and fundamental components during the negative half cycle.

International Scientific Journal of Engineering and Management (ISJEM) ISSN: 2583-6129
Volume: 05 Issue: 01 | Jan – 2026 DOI: 10.55041/ISJEM05344
An International Scholarly || Multidisciplinary || Open Access || Indexing in all major Database & Metadata

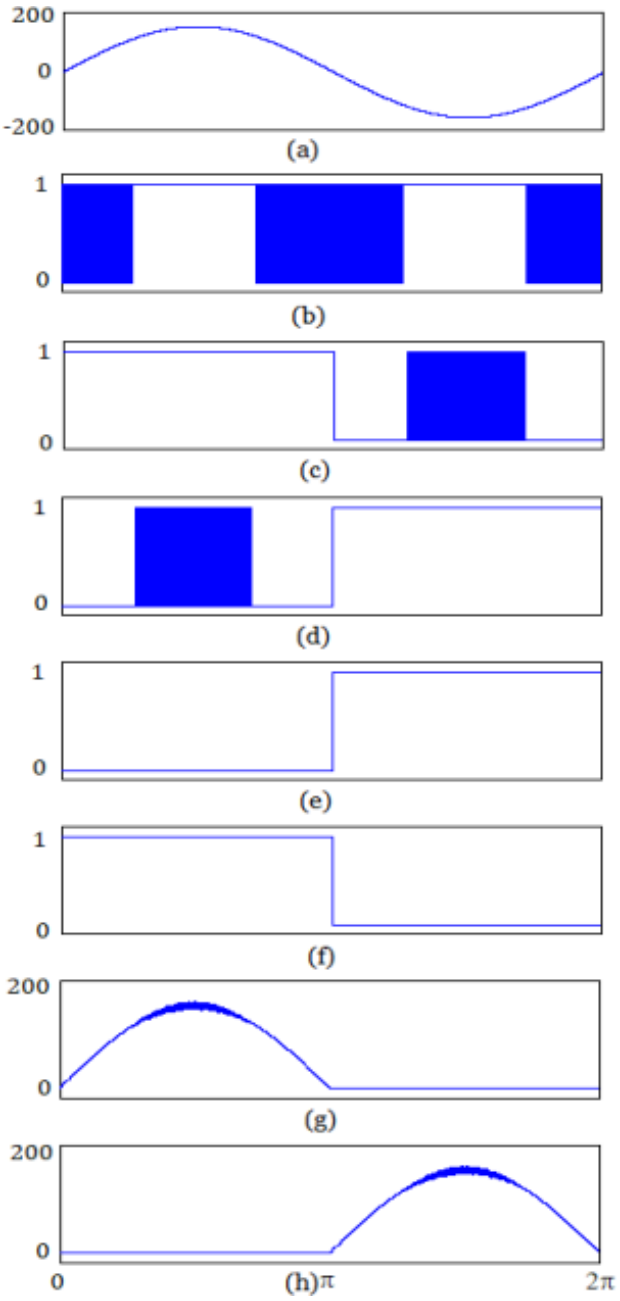

FIGURE 4. Control signals S1-S6 and operation voltage in a power grid cycle, (a) utility voltage, (b) S1, (c) S3, (d) S4, (e) S5, (f) S6, (g) VAN, (h) VBN.

V. OPERATION OF BPC

The bidirectional power converter (BPC) is placed between the solar array and the battery pack to regulate charging. It remains inactive when the solar power variation stays within a predefined limit. When this variation exceeds the limit, the BPC is activated to perform maximum power point tracking (MPPT). The converter operates in continuous conduction mode, establishing a defined relationship between the solar array voltage and the battery voltage.

$$\frac{V_{sol}}{V_{bat}} = \frac{1}{1 - D_{Sb}} \qquad (13)$$

where DSb is the duty cycle for Sb.

VI. SMOOTHING OPERATION

When the solar cell array output is stable, the DIBBDAI converts DC power to AC while tracking the maximum power point using the perturb and observe (P&O) method. Power smoothing is activated when the PV power variation (ΔPPV) exceeds a predefined limit P1. To protect battery life, the battery SOC is constrained between 30% and 90%, with a standby target of 60%. Since this work focuses on power smoothing, the SOC is estimated using the battery terminal voltage.

When ΔPPV exceeds +P1, MPPT control is shifted to the battery power conditioner (BPC), while the DIBBDAI linearly increases its output current according to a specified gradient, causing the SPGS output power (Pout) to rise smoothly. The excess power (PPV − Pout) is stored in the battery, increasing its SOC. Once Pout exceeds PPV by P2 (P2 ≤ P1), the DIBBDAI holds a constant output, and the battery supplies power to reduce SOC. If PPV stabilizes, smoothing stops when the SOC reaches 60%, and MPPT returns to the DIBBDAI. Smoothing is also disabled if the SOC reaches 90% to prevent overcharging.

Similarly, when ΔPPV drops below −P1, the DIBBDAI is powered by the battery, and Pout is linearly decreased along the specified gradient. The battery supplies the deficit power, reducing SOC. When Pout is sufficiently lower than PPV, the output is held constant and the battery is recharged. If PPV remains stable, smoothing stops once SOC returns to 60%. To avoid over-discharging, smoothing is disabled when SOC reaches 30%.

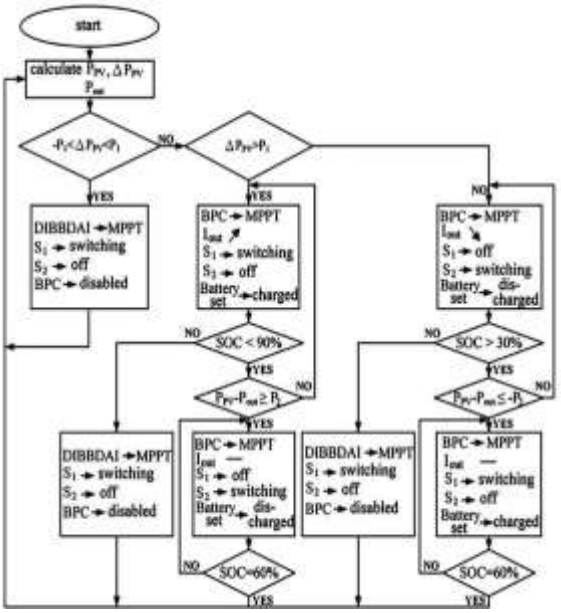

FIGURE 6. Operation flowchart for the proposed SPGS with power smoothing function.

As illustrated in Fig. 6, this strategy ensures that Pout varies smoothly along a predefined gradient during sudden PV power changes. Because the battery is used only when |ΔPPV| exceeds P1, the charging and discharging duration is shorter than in conventional methods [3]–[9]. Furthermore, the SOC is quickly restored to around 60% after smoothing, allowing a reduction in the required battery capacity.

International Scientific Journal of Engineering and Management (ISJEM) ISSN: 2583-6129
Volume: 05 Issue: 01 | Jan – 2026 DOI: 10.55041/ISJEM05344
An International Scholarly || Multidisciplinary || Open Access || Indexing in all major Database & Metadata

VII. CONTROL BLOCK

Fig. 7 illustrates the control structure of the DIBBDAI. The PV array voltage and current are fed to the MPPT block to compute PPV and predict the PV voltage. The predicted and measured voltages are processed by a PI controller to produce the MPPT control signal. The MPPT block also evaluates the power variation ΔPPV, which is compared with $\pm P1$ to generate the amplitude-gradient signal Ssl. When $\Delta P_{PV} > P1$, $Ssl = +Vsl$; when $\Delta PPV < -P1$, $Ssl = -Vsl$; otherwise, $Ssl = 0$.

The signal Ssl is integrated to create a linearly increasing or decreasing amplitude command, where Vsl sets the gradient of the output-current amplitude during power smoothing. Under steady PV power, $Ssl=0$ and the amplitude is governed solely by the MPPT signal. If P_{PV} varies significantly, the MPPT output is held constant while Vsl adjusts the amplitude gradient.

The amplitude command is multiplied by a unity sinusoidal signal to generate the current reference. This sinusoid is produced by a PLL and a sine table to ensure grid synchronization. Since the DIBBDAI operates in both buck and boost modes, the current controller is divided accordingly. In buck mode, the absolute value of the measured current is compared with the reference and processed by current controller I. Its output is combined with the feedforward term vf,bk to form the buck modulation signal, which is applied to PWM block I. Carrier-based PWM is used, where the modulation signal is compared with a triangular carrier to generate $PWMbk$.

$$v_{f,bk} = \frac{|v_s|}{k_{pwm1}} \tag{14}$$

and,

$$k_{pwm1} = \frac{V_{dc}}{V_{tri}} \tag{15}$$

Here, $Vtri$ is the peak of the triangular carrier, and Vdc is the input voltage of the DIBBDAI, from either the solar array or battery set. The DIBBDAI's output current in boost mode contains high-frequency harmonics, so the absolute current is filtered through a low-pass filter. The filtered current is compared with the reference and sent to current controller II. Its output, combined with the feedforward signal vf,bt, forms the boost modulation signal for PWM block II. Using carrier-based PWM, this modulation signal is compared with a triangular carrier to generate the boost PWM signal $PWMbt$. The feedforward signal vf,bt is:

$$v_{f,bt} = \frac{|v_s| - V_{dc}}{|v_s|} V_{tri} \tag{16}$$

The feedforward signals vf,bk and vf,bt form the main modulation, while current controllers I and II fine-tune it to ensure the output current accurately follows the reference sine wave. The grid voltage is compared with zero to generate Sp, which is 1 in the positive half-cycle and 0 in the negative. Its absolute value is also compared with Vdc to produce Sb; $Sb=1$ triggers boost mode, while $Sb=0$ triggers buck mode. Finally, Sp, Sb, PWMbk, and PWMbt are processed to generate control signals for switches S1–S6.

$$S_1 = (\bar{S}_b PWM_{bk} + S_b) \cdot S_o \tag{17}$$

$$S_2 = (\bar{S}_b PWM_{bk} + S_b) \cdot \bar{S}_o \tag{18}$$

$$S_3 = \bar{S}_p \cdot S_b \cdot PWM_{bt} + S_p \tag{19}$$

$$S_4 = S_p \cdot S_b \cdot PWM_{bt} + \bar{S}_p \tag{20}$$

$$S_5 = \bar{S}_p \tag{21}$$

$$S_6 = S_p \tag{22}$$

Here, So indicates the DIBBDAI input source, with 1 for solar array power and 0 for battery power. The BPC operates via current control using the MPPT signal from the solar array and the inductor Lb current. The current control output feeds the PWM block to generate the SD control signal.

VIII. EXPERIMENTAL RESULTS

The performance of the proposed SPGS was evaluated through simulations. The DIBBDAI output voltage was set at 100 V, producing a sinusoidal output current in phase with the grid voltage. In buck mode, the inductor current closely follows the output current, while in boost mode, it varies nonlinearly as a function of the duty cycle (D) of the switching device. Leakage current simulations with a 60 nF capacitor and 5 Ω resistor showed near-zero current during the positive half-cycle and minor high-frequency components in the negative half-cycle, yielding an RMS value of 10.15 mA, consistent with theoretical analysis.

In addition to power smoothing, the integration of IoT-based temperature monitoring introduces a crucial safety and intelligence layer. Continuous temperature sensing allows early detection of abnormal thermal conditions in system components, which is vital for preventing failures and fire-related hazards. IoT connectivity enables real-time data transmission and alerts through wireless networks, allowing timely user intervention and remote monitoring. [ambient temperature 20 to 46+ *C]

This system will provide safety notification in real-time over mobile sms, also user will be able to monitor the system temperature remotely via mobile phone.

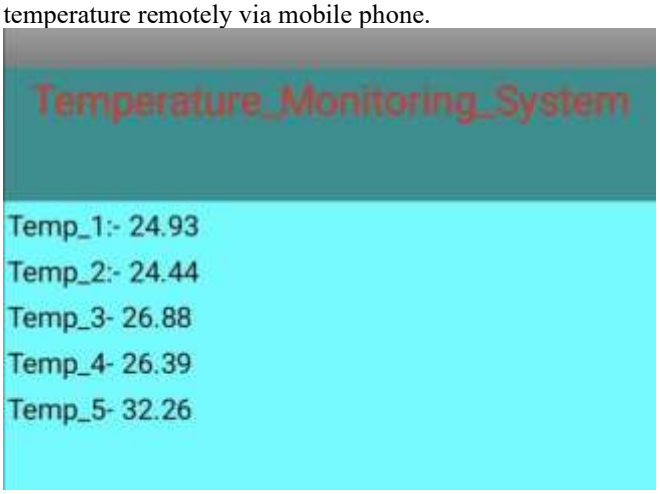

Fig : Snippet of Software [ThingSpeak IoT]

Compared to traditional monitoring approaches, IoT-based systems offer faster response, improved accuracy, and reduced

International Scientific Journal of Engineering and Management (ISJEM) ISSN: 2583-6129
Volume: 05 Issue: 01 | Jan – 2026 DOI: 10.55041/ISJEM05344
An International Scholarly || Multidisciplinary || Open Access || Indexing in all major Database & Metadata

false alarms while remaining cost-effective due to the availability of low-cost microcontrollers.

Overall, this project demonstrates a holistic approach by combining efficient solar power management with intelligent IoT-based temperature monitoring. The proposed system enhances energy reliability, operational safety, and system efficiency, making it well-suited for residential, commercial, and small-scale industrial renewable energy applications.

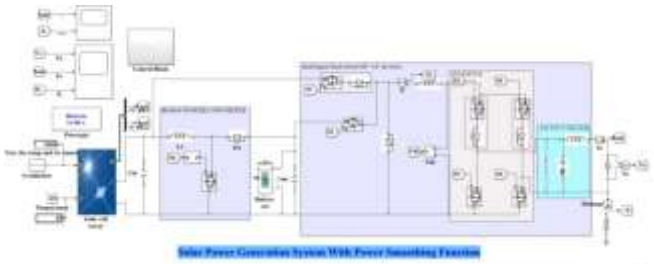

Fig 7: Schematic diagram

Simulations of varying input DC voltage from 87 V to 125 V revealed that the output current of the DIBBDA remains largely unaffected, though the inductor current peak decreases due to shorter boost intervals. Battery charging simulations with the BPC verified proper operation, while efficiency analysis showed higher input DC voltage leads to increased power efficiency.

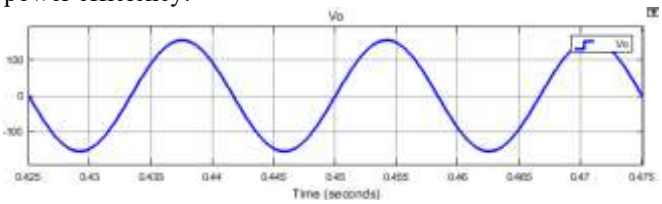

Fig 8: Output voltage

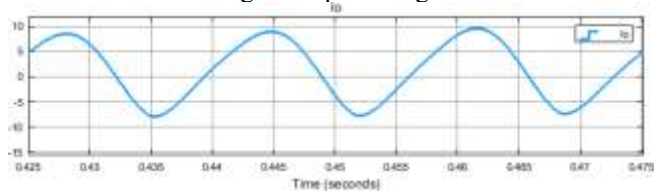

Fig 9: Output current

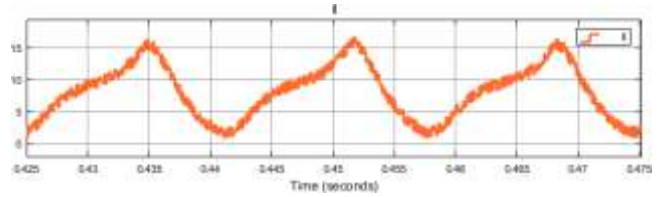

Fig 10: Inductor current

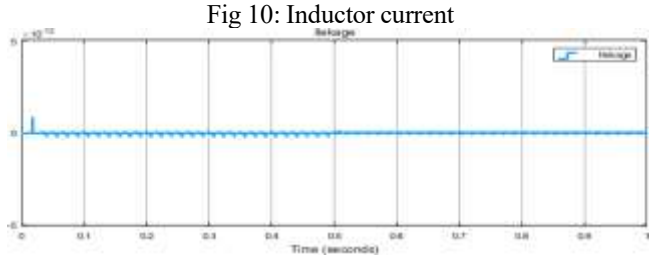

Fig 11 : I_lekage current

A PV simulator replicating three series-connected solar modules (255 W, 38.08 V, 8.65 A) was used to evaluate MPPT performance. The simulated solar power reached 550 W under 700 W/m² irradiance. When connected to the DIBBDA, the output power gradually stabilized at 550 W, demonstrating accurate MPPT tracking. Transient simulations examined abrupt solar power changes. For a sudden increase from 300 W to 500 W, the SPGS output followed a specified ramp (80 W/min), with excess power charging the battery. Conversely, a sudden drop from 500 W to 300 W caused the SPGS to discharge the battery to maintain output within the gradient, verifying effective power smoothing and battery coordination.

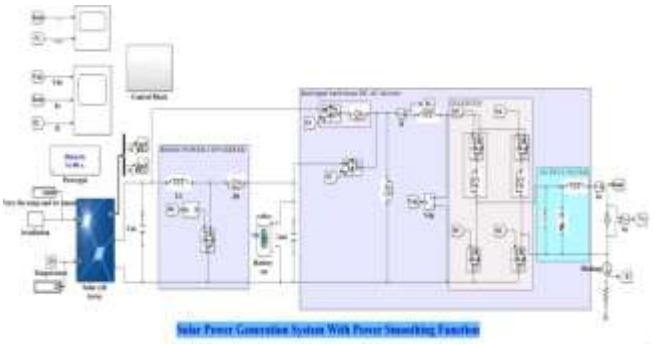

Fig 12: Schematic diagram for variable irradiation

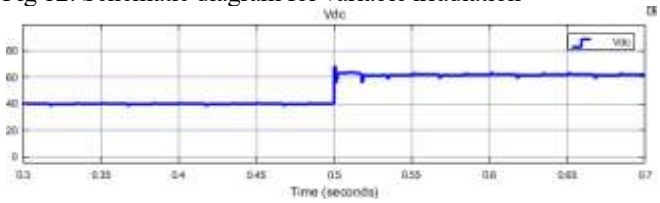

Fig 13: DC link voltage (Vdc)

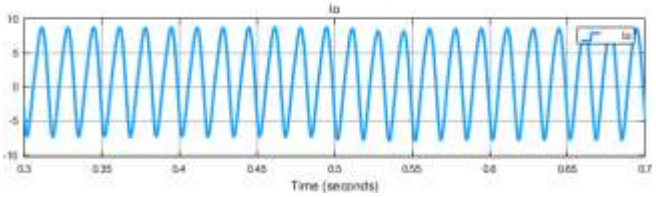

Fig 14: Output current (Io)

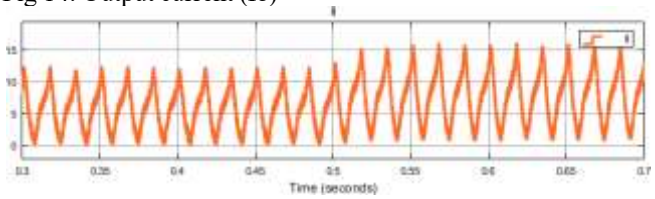

Fig 15: Inductor current

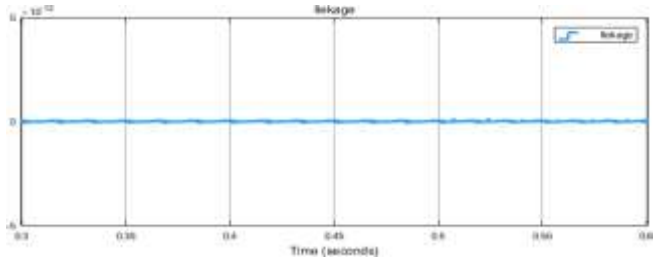

Fig 16: I_lekage current (I_lekage)

IX. CONCLUSION

This study presents a simulation of a Solar Power Generation System (SPGS) with a power smoothing function. The SPGS employs a DIBBDAI to coordinate the solar array and battery set for smoother power output. The system integrates two input sources, with the battery acting as an energy buffer to

mitigate solar power fluctuations. Only two power stages are used, simplifying the power circuit, and a single stage handles DC-to-AC conversion and battery charging.

Simulation results demonstrate that the SPGS delivers sinusoidal current in phase with the utility voltage and effectively smooths power variations from the solar array. Additionally, leakage current from stray capacitance is significantly reduced. These results confirm that the proposed SPGS can address both power fluctuation and leakage current issues. Further studies will evaluate battery capacity requirements and compare smoothing methods in practical applications.

REFERENCES

[1] Q.Peng,A.Sangwongwanich,Y.Yang,andF.Blaabjerg,''Grid-friendly power control for smart photovoltaic systems,'' Sol. Energy, vol. 210, pp. 115–127, Nov. 2020.

[2] D. Cheng, B. A. Mather, R. Seguin, J. Hambrick, and R. P. Broadwater, ''Photovoltaic (PV) impact assessment for very high penetration levels,'' IEEE J. Photovolt., vol. 6, no. 1, pp. 295–300, Jan. 2016.

[3] J.Martins,S.Spataru,D.Sera,D.-I.Stroe,andA.Lashab,''Comparative study of ramp-rate control algorithms for PV with energy storage systems,'' Energies, vol. 12, no. 7, p. 1342, Apr. 2019.

[4] D. Lin and N. Normal University, ''Strategy comparison of power ramp rate control for photovoltaic systems,'' CPSS Trans. Power Electron. Appl., vol. 5, no. 4, pp. 329–341, Dec. 2020.

[5] H. Nazaripouya, C.-C. Chu, H. R. Pota, and R. Gadh, ''Battery energy storage system control for intermittency smoothing using an optimized two-stage filter,'' IEEE Trans. Sustain. Energy, vol. 9, no. 2, pp. 664–675, Apr. 2018.

[6] K.Koiwa, K.-Z.Liu, and J.Tamura,''Analysisanddesignoffiltersforthe energy storage system: Optimal tradeoff between frequency guarantee and energy capacity/power rating,'' IEEE Trans. Ind. Electron., vol. 65, no. 8, pp. 6560–6570, Aug. 2018.

[7] M.J.E.Alam,K.M.Muttaqi,andD.Sutanto,''Anovelapproachforramp-rate control of solar PV using energy storage to mitigate output fluctuations caused by cloud passing,'' IEEE Trans. Energy Convers., vol. 29, no. 2, pp. 507–518, Jun. 2014.

[8] A. Atif and M. D. Khalid, ''Saviztky-Golay filtering for solar power smoothing and ramp rate reduction based on controlled battery energy storage,'' IEEE Access, vol. 8, pp.33806–33817, 2020.

[9] M. A. Syed and M. Khalid, ''Moving regression filtering with battery state of charge feedback control for solar PV firming and ramp rate curtailment,'' IEEE Access, vol. 9, pp.13198–13211, 2021.

[10] M. J. E. Alam, K. M. Muttaqi, and D. Sutanto, ''Battery energy storage to mitigate rapid voltage/power fluctuations in power grids due to fast variations of solar/wind outputs,'' IEEE Access, vol. 9, pp. 12191–12202, 2021.

[11] A. Makibar, L. Narvarte, and E. Lorenzo, ''Contributions to the size reduction of a battery used for PV power ramp rate control,'' Sol. Energy, vol. 230, pp. 435–448, Dec. 2021.

[12] M. Combe, A. Mahmoudi, M. H. Haque, and R. Khezri, ''Optimal sizing of an AC-coupled hybrid power system considering incentive-based demand response,'' IET Gener., Transmiss. Distrib., vol. 13, no. 15, pp. 3354–3361, Jul. 2019.

[13] V. T. Tran, M. R. Islam, D. Sutanto, and K. M. Muttaqi, ''Miti- gation of solar PV intermittency using ramp-rate control of energy buffer unit,'' IEEE Trans. Energy Convers., vol. 34, no. 1, pp. 435–449, Mar. 2019.

[14] S. Kumar, L. N. Patel, B. Singh, and A. L. Vyas, ''Self-adjustable step-based control algorithm for grid-interactive multifunctional single-phase PV-battery system under abnormal grid conditions,'' IEEE Trans. Ind. Appl., vol. 56, no. 3, pp. 2978–2987, May 2020.

[15] R. K. Dhar, A. Merabet, A. Al-Durra, and A. M. Y. M. Ghias, ''Power balance modes and dynamic grid power flow in solar PV and bat- tery storage experimental DC-link microgrid,'' IEEE Access, vol. 8, pp. 219847–219858, 2020.

[16] N.Vazquez,S.S.Yu,T.K.Chau,T.Fernando,andH.H.-C.Iu,''Afully decentralized adaptive droop optimization strategy for power loss mini-mization in microgrids with PV-BESS,'' IEEE Trans. Energy Convers., vol. 34, no. 1, pp. 385–395, Mar. 2019.

[17] C. M. Nirmal Mukundan, P. Jayaprakash, U. Subramaniam, and D. J. Almakhles, ''Binary hybrid multilevel inverter-based grid integrated solar energy conversion system with damped SOGI control,'' IEEE Access, vol. 8, pp. 37214–37228, 2020.

[18] J. Wu, H. Jou, and X. Wu, ''Power conversion interface with harmonic suppression for a DC grid and single-phase utility,'' IET Power Electron., vol. 13, no. 7, pp. 1302–1310, May 2020.

[19] D.Ghaderi,G.Bayrak,andJ.M.Guerrero,''Gridcodecompatibilityand real-time performance analysis of an efficient inverter topology for PV-based microgrid applications,'' Int. J. Electr. Power Energy Syst., vol. 128, Apr. 2021, Art. no. 106712.

[20] E. Kabalcè, ''Review on novel single-phase grid-connected solar invert- ers: Circuits and control methods,'' Sol. Energy, vol. 198, pp. 247–274, Mar. 2020.

[21] A. Sangwongwanich, Y. Yang, and F. Blaabjerg, ''A sensorless power reserve control strategy for two-stage grid-connected PV systems,'' IEEE Trans. Power Electron., vol. 32, no. 11, pp. 8559–8569, Nov. 2017.

[22] A. Sinha, K. C. Jana, and M. K. Das, ''Control strategy of PV-fed, grid-interfaced, seven-level T-type MLI for distributed power generation,'' IET Power Electron., vol. 12, no. 12, pp. 1–12, Jul. 2019.

[23] J. C. Wu, H. L. Jou, and P. H. Huang, ''Seven-level power conversion system for solar power generation system,'' IET Renew. Power Gener., vol. 14, no. 8, pp. 1387–1394, Jun. 2020.

[24] Y. He, Y. Xu, and J. Chen, ''New space vector modulation strategies to reduce inductor current ripple of Z-source inverter,'' IEEE Trans. Power Electron., vol. 33, no. 3, pp. 2643–2654, Mar. 2018.

[25] W. Xu, M. Liu, J. Liu, K. W. Chan, and K. W. E. Cheng, ''A series of new control methods for single-phase Z-source inverters and the optimized operation,'' IEEE Access, vol. 7, pp. 113786–113800, 2019.

[26] S.Huang,F.Tang,Z.Xin,Q.Xiao,andP.C.Loh,''Grid-currentcontrolof a differential boost inverter with hidden LCL filters,'' IEEE Trans. Power. Electron., vol. 34, no. 1, pp. 889–903, Jan. 2019.

[27] W.Yao,Y.Xu,Y.Tang,P.C.Loh,X.Zhang,andF.Blaabjerg,''General-ized power decoupling control for single-phase differential inverters with nonlinear loads,'' IEEE J. Emerg. Sel. Topics Power Electron., vol. 7, no. 2, pp. 1137–1151, Jun. 2019.

[28] A.A.Khan,Y.W.Lu,W.Eberle,L.Wang,U.A.Khan,M.Agamy,and H. Cha, ''Single-stage bidirectional buck–boost inverters using a single inductor and eliminating the common-mode leakage current,'' IEEE Trans. Power Electron., vol. 35, no. 2, pp. 1269–1281, Feb. 2020.

[29] A.A.Khan,Y.W.Lu,U.A.Khan,L.Wang,W.Eberle,andM.Agamy, ''Novel transformerless Buck–Boost inverters without leakage current,'' IEEE Trans. Ind. Electron., vol. 67, no. 12, pp. 10442–10454, Dec. 2020.

[30] U.A.KhanandJ.-W.Park,''Full-bridgesingle-inductor-basedbuck–boost inverters,'' IEEE Trans. Power Electron., vol. 36, no. 2, pp. 1909–1920, Feb. 2021.

[31] O. Husev, O. Matiushkin, C. Roncero-Clemente, F. Blaabjerg, and D. Vinnikov, ''Novel family of single-stage buck–boost inverters based on unfolding circuit,'' IEEE Trans. Power Electron., vol. 34, no. 8, pp. 7662–7676, Aug. 2019.

[32] O. Matiushkin, O. Husev, J. Rodriguez, H. Young, and I. Roasto, ''Feasi- bility study of model predictive control for grid-connected twisted buck– boost inverter,'' IEEE Trans. Ind. Electron., vol. 69, no. 3, pp. 2488–2499, Mar. 2022.

[33] M. N. H. Khan, M. Forouzesh, Y. P. Siwakoti, L. Li, T. Kerekes, and F. Blaabjerg, ''Transformerless inverter topologies for single-phase photo- voltaic systems: A comparative review,'' IEEE J. Emerg. Sel. Topics Power Electron., vol. 8, no. 1, pp. 805–835, Mar. 2020.

[34] H. Sabry, Z. M. Mohammed, F. H. Nordin, N. H. N. Ali, and A. S. Al-Ogaili, ''Single-phase grid-tied transformerless inverter of zero leakage current for PV system,'' IEEE Access, vol. 8, pp. 4361–4371, 2020..